La radiologia medica (2020) 125:365–373
https://doi.org/10.1007/s11547-020-01179-x

CHEST RADIOLOGY

# Proposal of a low-dose, long-pitch, dual-source chest CT protocol on third-generation dual-source CT using a tin filter for spectral shaping at 100 kVp for CoronaVirus Disease 2019 (COVID-19) patients: a feasibility study

**Andrea Agostini[1,2] · Chiara Floridi[1,2] · Alessandra Borgheresi[2] · Myriam Badaloni[2] · Paolo Esposto Pirani[2] · Filippo Terilli[2] · Letizia Ottaviani[2] · Andrea Giovagnoni[1,2]**

Received: 9 March 2020 / Accepted: 18 March 2020 / Published online: 1 April 2020


## Abstract

**Aim** To subjectively and objectively evaluate the feasibility and diagnostic reliability of a low-dose, long-pitch dual-source chest CT protocol on third-generation dual-source CT (DSCT) with spectral shaping at 100Sn kVp for COVID-19 patients.

**Materials and methods** Patients with COVID-19 and positive swab-test undergoing to a chest CT on third-generation DSCT were included. The imaging protocol included a dual-energy acquisition (HD-DECT, 90/150Sn kVp) and fast, low-dose, long-pitch CT, dual-source scan at 100Sn kVp (LDCT). Subjective (Likert Scales) and objective (signal-to-noise and contrast-to-noise ratios, SNR and CNR) analyses were performed; radiation dose and acquisition times were recorded. Nonparametric tests were used.

**Results** The median radiation dose was lower for LDCT than HD-DECT (Effective dose, ED: 0.28 mSv vs. 3.28 mSv, $p=0.016$). LDCT had median acquisition time of 0.62 s (vs 2.02 s, $p=0.016$). SNR and CNR were significantly different in several thoracic structures between HD-DECT and LDCT, with exception of lung parenchyma. Qualitative analysis demonstrated significant reduction in motion artifacts ($p=0.031$) with comparable diagnostic reliability between HD-DECT and LDCT.

**Conclusions** Ultra-low-dose, dual-source, fast CT protocol provides highly diagnostic images for COVID-19 with potential for reduction in dose and motion artifacts.

**Keywords** COVID-19 · 2019-nCOV · Dual-source CT · Spectral shaping · Low-dose CT · Chest radiology

## Introduction

In December 2019, a pneumonia of unknown origin outbreak in Wuhan, Hubei province (China); the responsible pathogen was identified as the novel coronavirus (2019-nCOV), and the related pulmonary syndrome was named as COVID-19 (CoronaVirus Disease 2019) by the *World Health Organization* (WHO) [1, 2]. Common presenting clinical symptoms are fever and cough in addition to other unspecific symptoms including, fatigue, dyspnea, muscle soreness and headache [3]. Intriguingly, a small percentage (5%) case is asymptomatic (i.e., with normal body temperature or minor discomfort) [4, 5], while reverse-transcription polymerase chain reaction (RT-PCR) from swab samples has demonstrated high specificity but relatively low sensitivity (60–70%) [6, 7]. Moreover, when comparing RT-PCR to chest CT, the latter demonstrated a better sensitivity in particular in early stages [6, 7]. Therefore, the RT-PCR from swab samples is still the standard of reference in the diagnosis of COVID-19, while unenhanced, high-resolution chest computed tomography (CT) has a central role in detection, diagnosis and follow-up of the disease [8–10].

CT is a widely available technique allowing for high-quality and standardized evaluation of the lung parenchyma.

✉ Alessandra Borgheresi
alessandra.borgheresi@gmail.com

[1] Department of Clinical, Special and Dental Sciences, University Politecnica delle Marche, Ancona, AN, Italy

[2] Division of Special and Pediatric Radiology, Department of Radiology, University Hospital "Umberto I – Lancisi – Salesi", Via Conca 71, 60126 Ancona, AN, Italy

However, radiation exposure and motion artifacts are major issues in uncooperative, young patients undergoing to repeated CT examinations [11]. To reduce motion artifacts in uncooperative patients (e.g., pediatric patients or patients with dyspnea), fast acquisitions are obtained by lowering the rotation time of the tube-detector system with high pitch and wide collimation values [12]. Conversely, lower radiation doses are achieved at low kV with the implementation of iterative reconstructions for noise reduction [13]. The dual-source CT scanners (DSCT, Siemens Healthineers, Erlangen, Germany) are equipped with two asymmetrical tube-detector systems (i.e., different scan Field of View, FOV), mounted in the gantry with an offset of ~ 90°. The two tube-detector systems work at different kVp settings for dual-energy acquisitions or at the same kVp setting for ultrafast acquisitions at long pitch (Pitch 1.5–3, Flash or Turbo Flash mode, Siemens Healthineers, Erlangen) [14, 15]. Moreover, the X-ray tubes in the second- and third-generation scanners (respectively, the Somatom Flash and Force, Siemens Healthineers, Erlangen) have additional tin filtration [16, 17]. In particular, the more aggressive tin filtration in the Somatom Force provides the best spectral separation in dual-energy (DECT) acquisitions by increasing the mean energy of high-kVp spectrum (i.e., 150Sn kVp) [17]. Moreover, the spectral shaping with tin filter (i.e., 100Sn kVp) allows for reduction in the low-energy component of the X-ray spectrum, leading to significant dose reduction [18, 19]. Coupling an ultra-low-dose, fast, long-pitch dual-source acquisition with spectral shaping may be of relevant value in serial evaluations in dyspneic or coughing patients with COVID-19.

The aim of this work is to test the feasibility, with subjective and objective analysis, of an ultra-low-dose, fast, long-pitch, dual-source acquisition on third-generation DSCT (Somatom Force, Siemens Healthineers, Erlangen) for the lung evaluation in patients affected by COVID-19 related pneumonia.

## Materials and methods

### Ethical standards

This study was approved by the local Ethical Board, and the informed consent was not collected in written form because of the specific disease.

### Patient population

Inpatients > 18 years old, positive for COVID-19 of the upper respiratory tract swab from the Division of Infectious Disease, referred to the Department of Radiology for a chest high-resolution CT between Feb 24, 2020 and March 4, 2020, with no basal chest X-ray performed, were prospectively included to be scanned on the third-generation DSCT (Somatom Force, Siemens Healthineers). Anamnestic and clinical information were collected. Patients with pneumonia other than COVID-19, or with contraindication to CT were excluded.

### Image acquisition and reconstruction

The imaging protocol on the third-generation DSCT (Somatom Force, Siemens Healthineers, Erlangen) was composed by a spiral high-resolution dual-energy acquisition (HD-DECT) and by an ultra-low-dose acquisition (LDCT) in deep inspiration when possible; no contrast material was administered. Since COVID-19 pathological mechanism is not completely understood, and other strains of coronavirus family demonstrated similar pulmonary syndromes with development of fibrosis (i.e., air trapping); the first three patients were evaluated also with an ultra-low-dose, fast scan in deep expiration [20, 21].

A relatively fast DECT, spiral, caudocranial acquisition (HD-DECT) was set with the following parameters: 90/150Sn kVp, modulated mA (CareDose 4D, Siemens Healthineers, Erlangen, Germany) with reference 85 mAs, rotation time 0.25 s, a relatively long pitch of 1.1 and a wide collimation ($2 \times 192 \times 0.6$ mm). In the ultra-low-dose, fast acquisition (LDCT), both the tubes worked at 100 kVp with 0.6-mm tin filter (100Sn kVp), with a wide collimation ($2 \times 192 \times 0.6$ mm), a rotation time of 0.25 s, an ultra-long pitch (pitch = 3, TurboFlash mode, Siemens Healthineers), with modulated mA at 180 mAs reference.

Both the HD-DECT and LDCT datasets were reconstructed with the available iterative reconstruction algorithm ADMIRE, Strength 4 (Advanced Modeled Iterative Reconstruction, Siemens Healthineers, Erlangen). The lung parenchyma was reconstructed with sharp kernels (HD-DECT: Bl64; LDCT: Bl57), with linear blending of 0.7 at slice thickness/spacing of 1.5/1 mm and a window/level of 1200/-600 HU (named Lung Images, LUNG). The mediastinal structures were evaluated with softer kernel (Br40 for both acquisitions) with linear blending of 0.7, slice thickness/spacing of 3/1.5 mm and a window/level of 350/50 HU (named Mediastinal Images, MED). Sagittal and coronal reconstructions were obtained.

DECT datasets were reconstructed with different linear blending ratios (Blending Ratio 0.2) in order to reduce beam-hardening artifacts in uncooperative patients on a dedicated workstation (Syngo.via VA20, Dual Energy, Siemens Healthineers, Erlangen).

### Radiation Dose evaluation and Acquisition Time

The CT dose index (CTDIvol) and dose length product (DLP) for each scanned patient were recorded. The effective dose (ED) was calculated using a conversion factor ($k$) of 0.0145 $mSv \times mGy^{-1} \times cm^{-1}$ for 120 kV according to Deak et al. [22] based on the following formula:

$$ED = DLP \times k$$

Finally, the acquisition (exposure) times for HD-DECT and LDCT were recorded.

### Subjective image analysis

Two independent radiologists with 15 and 10 years of experience evaluated the quality of the CT images on a PACS workstations (Picture Archiving and Communication System; Centricity Radiology, GE Healthcare, Milwaukee), after removing personal and technical data from the images. The lung parenchyma and airways were evaluated on Lung Images, while the mediastinal structures (e.g., lymph nodes) were evaluated on the Mediastinal Images, in HD-DECT and LDCT.

The subjective analysis was performed by using 5-points Likert scale and included three sections: general quality of the image (mediastinum and lung images), anatomical structures (lung images), pathological findings (lung or mediastinal images).

The evaluation of general quality included the following parameters and scales:

1. Sharpness, where sharpness was rated as: 1 = unacceptable, 2 = significantly reduced with blurring of adjacent structures, 3 = minimally reduced sharpness with blurring of adjacent structures, 4 = sharpness minimally reduced, 5 = excellent sharpness;
2. Perceived image noise: 1 = unacceptable, 2 = above average, 3 = average image, 4 = less than average, 5 = minimal;
3. Motion artifacts: 1 = unacceptable, non-diagnostic; 2 = marked; 3 = mild; 4 = minimal; 5 = no motion artifacts
4. Subjective diagnostic reliability: 1 = no diagnostic significance; 2 = poor; 3 = fair; 4 = good; 5 = optimal diagnostic reliability;
5. Overall image quality, including other artifacts—beam-hardening artifacts: 1 = unacceptable, 2 = fair, 3 = moderate, 4 = good, 5 = excellent.

The evaluation of anatomic structures included the parameters:

1. Major anatomical structures (fissures and small vessels);
2. Small anatomical structures (bronchi < 2 mm and septae);

In both cases, the Likert scale was defined as follows: 1 = unacceptable (landmarks not visible); 2 = poor (< 25% landmarks visible); 3 = fair (25–75% landmarks visible); 4 = good (> 75% landmarks visible); 5 = excellent (all landmarks visible).

Finally, a third radiologist (10 years of experience) detected main lung pathological findings related to COVID-19 on HD-$DECT_{LUNG}$ and HD-$DECT_{MED}$ images and the other two radiologists were asked to evaluate the same finding on the ultra-low-dose acquisitions, in particular:

1. Ground glass opacities (GGO) (< 20 mm);
2. COVID-19 signs, e.g., reverse halo/crazy paving;
3. Centrolobular nodules;
4. Consolidations (segmental–subsegmental);
5. Lymph nodes (on HD-$DECT_{MED}$);

The relative Likert scale was set as follows: 1 = finding not detected; 2 = barely detected, unreliable interpretation; 3 = visible finding with marked blurring and uncertain interpretation; 4 = visible finding, blurred, with no influence on diagnosis; 5 = finding clearly visible with good demarcation.

### Objective image analysis

Signal-to-noise ratio (SNR) and contrast-to-noise ratio (CNR) were evaluated by the third radiologist (10 years of experience) by placing $1 \pm 0.05$ $cm^2$ circular Region of Interest (ROI) for the following structures:

1. SNR:
   a. HD-$DECT_{LUNG}$ and $LDCT_{LUNG}$: lung parenchyma, trachea and muscle and subcutaneous fat;
   b. HD-$DECT_{MED}$ and $LDCT_{MED}$: trachea, descending aorta, paraspinal muscle, subcutaneous fat;

2. CNR (the selected reference was the subcutaneous fat):
   a. HD-$DECT_{LUNG}$ and $LDCT_{LUNG}$: lung parenchyma, trachea, paraspinal muscle;
   b. HD-$DECT_{MED}$ and $LDCT_{MED}$: descending aorta, trachea, paraspinal muscle.

SNR and CNR were calculated considering average and standard deviation (SD) of the HU from the placed ROI as follows [13]:

$$SNR = \frac{\left|\text{Average HU}_{\text{Anatomical Structure}}\right|}{\text{SD}_{\text{Anatomical Structure}}}$$

$$CNR = \frac{\left|\text{Average HU}_{\text{Anatomical Structure}} - \text{Average HU}_{\text{fat}}\right|}{\text{SD}_{\text{fat}}}$$

### Statistical analysis

Quantitative parameters were expressed as median and interquartile ranges (25–75 p, IQR). Qualitative and quantitative parameters were compared with nonparametric tests (Wilcoxon for paired samples). A dedicated statistical software was used (MedCalc v19.1.6, MedCalc Software, Ostend, Belgium).

**Table 1** Main radiological findings in 10 COVID-19 positive patients

| Radiological finding | Number of patients: 10 |
|---|---|
| Ground glass opacities | 10 (100%) |
| *Multiple and Bilateral* | 10 (100%) |
| *with consolidation* | 7 (70%) |
| Linear opacities | 7 (70%) |
| Rounded opacities | 2 (20%) |
| Peripheral involvement | 10 (100%) |
| Central parenchyma involvement | 1 (10%) |
| "Crazy-Paving" pattern | 3 (30%) |
| "Reverse Halo" Sign | 2 (20%) |
| Bronchial Wall Thickening | 5 (50%) |
| Bronchiectasis | 4 (40%) |
| Lymphadenopathy | 0 |
| Bilateral lung involvement | 9 (90%) |
| > 2 lobes affected | 8 (8%) |
| Air trapping | 0 |

## Results

### Patient Population and radiological findings on CT

In this study were included 10 patients (M/F = 7/3) with a median age of 53 (IQR: 47–83) and a median BMI of 28 (IQR: 26–30). Two of 10 patients (20%) had a BMI > 30 and 3/10 (39%) had severe symptoms (Temperature > 38 °C, dyspnea and respiratory failure) and were not able to maintain the arms raised during the CT examination. The radiological findings of each patient at presentation are summarized in Table 1 and are comparable to those previously reported [8].

### Radiation dose and acquisition time

Table 2 summarizes the applied radiation dose and acquisition time. Statistically significant differences were found in radiation dose and acquisition times. The use of spectral shaping at 100 kV (100Sn kVp) allowed for a significant reduction in ED, with a median dose reduction of 90.6% (−88.35 to −91.12%).

### Objective image analysis

The results of the objective image quality analysis are shown in Table 3. Statistically significant differences were found in SNR and CNR, with higher values in HD-DECT images, for different anatomical structure with exception of lung parenchyma ($p > 0.05$).

### Subjective image analysis

The results of the subjective image evaluation assessment are summarized in Table 4. On the basis of the average Likert scale, the two radiologists assessed for the overall subjective image quality a median point value of 4 for both the protocols. As expected, the subjective image noise had a trend to be worse in the LDCT. However, the LDCT demonstrated a significant reduction in the motion artifacts when compared to the standard DECT (4 vs. 5) (Fig. 1a, b). Nevertheless, in terms of diagnostic

**Table 2** Radiation dose and exposure times

| | HD-DECT median (25 - 75 p) | LDCT median (25 - 75 p) | *P** |
|---|---|---|---|
| CTDIvol (mGy) | 6.38 (3.91–7.51) | 0.64 (0.47–1.12) | 0.016 |
| DLP (mGy × cm) | 226.21 (176.01–322.03) | 19.5 (17.5–29.02) | 0.016 |
| ED (mSv) | 3.28 (2.55–4.67) | 0.28 (0.25–0.42) | 0.016 |
| Exposure time (s) | 2.02 (1.81–2.36) | 0.62 (0.54–0.72) | 0.016 |

*CTDI* CT dose index; *DLP* dose length product; *ED* effective dose

*Wilcoxon test for paired samples

**Table 3** Objective image analysis: signal-to-noise (SNR) and contrast-to-noise (CNR) ratios

| | $HD\text{-}DECT_{LUNG}$ Median (25–75 p) | $LDCT_{LUNG}$ Median (25–75 p) | *P** | $HD\text{-}DECT_{MED}$ Median (25–75 p) | $LDCT_{MED}$ Median (25–75 p) | *P** |
|---|---|---|---|---|---|---|
| *SNR* | | | | | | |
| Descending aorta | // | // | – | 4.06 (3.44–5.51) | 1.84 (1.72–2.22) | 0.016 |
| Lung parenchyma | 13.49 (12.76–17.48) | 12.2 (9.83–14.21) | 0.578 | // | // | – |
| Trachea | 24.52 (16.67–40.29) | 19.9 (14.33–20.84) | 0.219 | 29.38 (12.64–94.91) | 41.93 (19.34–56.52) | 0.038 |
| Subcutaneous fat | 2.37 (1.34–2.67) | 0.98 (0.93–1.22) | 0.016 | 10.53 (9.85–12.15) | 4.82 (4.43–6.03) | 0.016 |
| Muscle | 0.65 (0.46–0.77) | 0.44 (0.25–0.52) | 0.016 | 3.83 (1.13–4.14) | 1.7 (0.82–2.25) | 0.047 |
| *CNR* | | | | | | |
| Descending aorta | // | // | – | 14.35 (12.93–16.29) | 6.66 (6.11–8.61) | 0.016 |
| Lung parenchyma | 15.63 (8.48–18.89) | 7.54 (76.82–9.68) | 0.057 | // | // | – |
| Trachea | 17.4 (9.35–20.21) | 8.21 (7.56–10.29) | 0.047 | 78.68 (73.25–93.24) | 40.70 (35.17–53.28) | 0.016 |
| Muscle | 3.00 (1.72–3.87) | 1.48 (1.33–1.74) | 0.016 | 15.21 (11.81–15.42) | 7.18 (6.56–7.26) | 0.016 |

**Table 4** Subjective image analysis with Likert scales (see text)

| | HD-DECT Median (25–75 p) | LDCT Median (25–75 p) | *P** |
|---|---|---|---|
| *General evaluation* | | | |
| Image sharpness | 4 (4–4) | 4 (4–4) | – |
| Additional image noise | 4 (4–5) | 4 (3–4) | 0.063 |
| The presence of motion artifacts | 4 (2–4) | 5 (5–5) | 0.031 |
| Subjective diagnostic reliability | 5 (4–5) | 5 (4–5) | – |
| Overall diagnostic image quality | 4 (4–5) | 4 (4–5) | – |
| *Anatomy* | | | |
| normal lung structures (major fissures and small vessels) | 5 (5–5) | 5 (4–5) | – |
| bronchi (< 2 mm diameter) | 5 (4–5) | 5 (4–5) | – |
| *Parenchymal findings* | | | |
| GGO < 2 cm | Reference standard | 5 (4–5) | // |
| COVID signs (Crazy paving—reverse Halo sign) | Reference standard | 5 (4–5) | // |
| Centrolobular nodules | Reference standard | 3 (3–4) | // |
| lobar/subsegmental consolidations | Reference standard | 5 (4–5) | // |
| Lymphadenopathy | Reference standard | 4 (4 –5) | // |

Median values on the Likert scale (from 1 unacceptable to 5 excellent) for the two readers

* Wilcoxon test for paired samples

– Unable to calculate p

// Test not performed

performance the radiologist did not experience a significant reduction in diagnostic reliability and evaluation of the pathological findings between the two protocols (Fig. 2a–c).

Finally, post-processing of DECT datasets at different blending ratio allowed for reduction in beam-hardening artifacts in 1/10 (10%) patients who was unable to maintain the arms raised (Fig. 1c–f). The beam-hardening artifacts minorly affected the 100Sn kV.

## Discussion

In the present study, we included a small sample of patients affected by COVD-19-related pneumonia with variable clinical and radiological manifestation of the disease, and comparable findings described in the literature [8, 9]. Given the etiological and clinical similarities between COVID-19 and other pulmonary syndromes such

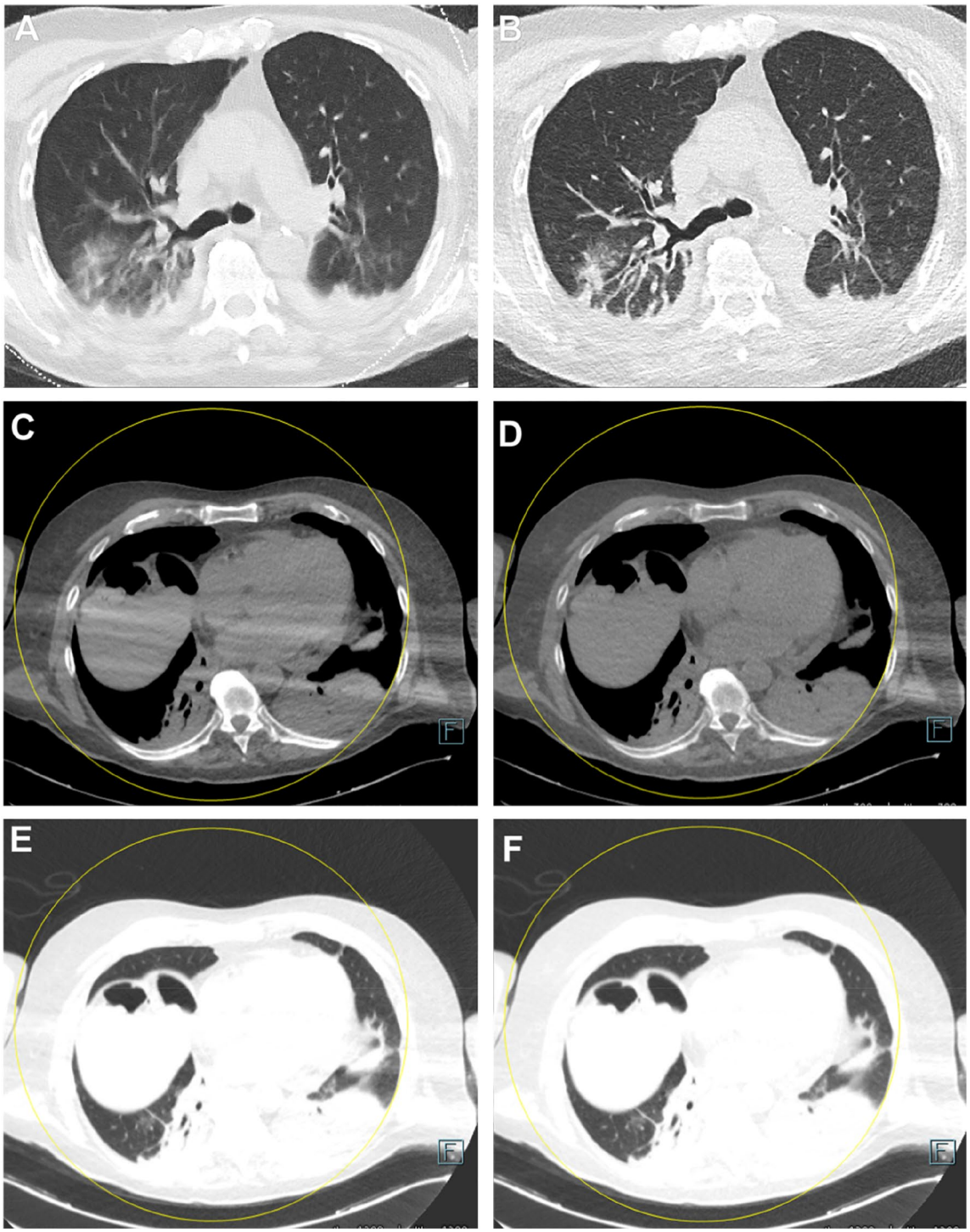


**Fig. 1** Technical advantages of DECT and LDCT. Axial images, **a**, **c**, **d**, **e**, **f**: HD-DECT; **b**: LDCT, lung kernel. **a**, **b** Comparison of HD-DECT and LDCT, demonstrating the reduction in the motion artifact in the LDCT. **c**–**f** Shows the role of DECT in reduction in beam-hardening artifacts. **c**, **e** have a linear blending of 0.7 while D, F have linear blending of 0.2 resulting in reduction in artifacts in mediastinum (**d**) and left lung parenchyma (**f**)

as SARS and MERS (which demonstrated the development of air trapping and fibrosis [21]), the presence of air trapping was searched in the first three cases, with negative results and thus not investigated any more. Further studies on follow-up of COVID-19 should be performed to clarify possible chronic lung injuries.

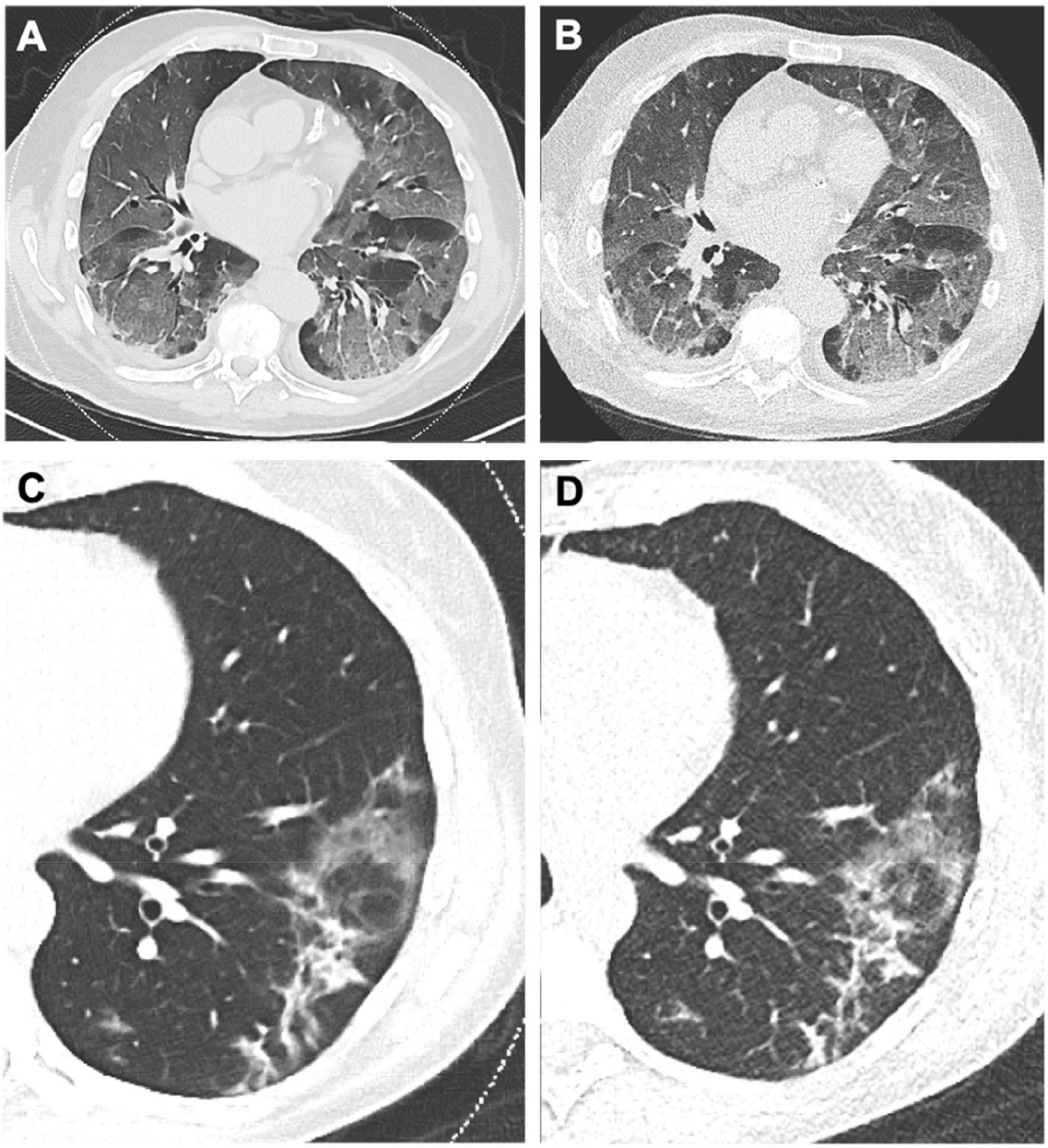


**Fig. 2** COVID-19 Pathological Findings: HD-DECT versus LDCT. Axial Images. **a**, **c** HD-DECT; **b**, **d** LDCT. **a**, **b** Good demonstration of crazy-paving both in **a** and **b**. **c**, **d** demonstration of Reverse Halo and linear opacities in HD-DECT and LDCT

In these 10 patients with COVID-19, we evaluated the feasibility of an ultra-low-dose, long-pitch, dual-source, fast CT acquisition to be implemented for serial follow-up examinations in symptomatic patients with COVID-19. At baseline, a DECT acquisition was chosen as internal reference standard.

Previous studies in the literature demonstrated significant dose reduction with spectral shaping in chest CT, achieving a dose comparable to a chest x-ray examination [12, 13, 18, 19, 23, 24]. In our population, the effective dose of the ultra-low-dose, long-pitch, dual-source fast acquisition was comparable to the values reported in previous studies and close to a chest X-ray examination. In these patients, chest X-ray examination at baseline was not performed to avoid unnecessary radiation exposure.

The rationale behind the DECT choice was to couple a relatively fast acquisition (2–2.5 s) with the possibility of post-processing for eventual artifact reduction with different blending combinations in uncooperative patients unable to maintain arms raised. The post-processing of DECT datasets reduced beam-hardening artifacts in 1/10 patients (10%). These artifacts minorly affected the LDCT. An explanation of this can

be found in the relatively high mean energy of the 100Sn kVp spectrum [19].

Conversely, the LDCT acquisition was conceived to avoid artifacts from heart beats, breathing and coughing in patients with severe symptoms, which was significantly demonstrated in the subjective analysis (Table 4, Fig. 1). The feasibility, the quality and the diagnostic performance of ultra-low-dose chest CT with spectral shaping, and other technical solutions have already been demonstrated [12, 13, 18, 19, 24] sometimes with questionable results about the pathological findings [25]. To our knowledge, this is the first study evaluating a long-pitch, dual-source acquisition with spectral shaping in acute setting in patients with COVID-19. As expected from a low-dose acquisition, the LDCT images had trend, though poorly significant, to be evaluated as more noisy than the HD-DECT images (Table 4). However, it did not significantly influence the detection and characterization of main anatomical and pathological pulmonary findings in this subset of patients, as demonstrated by the high rankings (Likert $\geq 3$ for the pathological findings in Table 4) (Fig. 2).

The quantitative analysis found significant differences in SNR and CNR for several anatomical structures, as expected when comparing a standard-dose and an ultra-low-dose acquisition with an ultra-long pitch. However, these differences had poor significance in the evaluation of lung SNR and CNR, in agreement to the subjective analysis. Again, this can be explained by considering the relatively high mean energy of the 100Sn kVp spectrum contributing to lowering the noise together with the radiation dose (Table 2, Fig. 2) [19]. Moreover, in this protocol, the reconstructions have been kept as similar as possible, in particular the slice thickness, the slice spacing and the iterative reconstructions while for LDCT a slightly softer kernel was used. Again, in Table 4, the image sharpness of LDCT was comparable with maintained diagnostic reliability. Further studies are necessary to fully explore the role of iterative reconstructions at lower doses in this acute setting [18].

The study has several limitations. It is a single-center study with a small population to evaluate the feasibility of a low-dose CT protocol in acute setting. The small size of the sample did not allow for more sophisticated statistical analysis, such as inter-reader agreement or the relation between BMI, radiation dose and image quality.

Concluding, a compromise including preserved image sharpness within lung parenchyma, with minimally blurred mediastinal structures in the face of a median dose reduction of more than 90% may be acceptable when performing serial CT controls in severely ill young patients [26].

## Conclusions

The study demonstrated the feasibility of an ultra-low-dose, fast chest CT acquisition with spectral shaping at 100 kVp (100Sn kV) and dual-source acquisition with ultra-long pitch (Turbo Flash, Siemens Healthineers) in patients affected by COVID-19 with good diagnostic reliability and potential for reduction in radiation dose and motion artifacts.

**Funding** This study was not supported by any funding.

### Compliance with ethical standards

**Conflict of interest** A.A. is a speaker for Siemens Helthineers. The other authors declare that they have no conflict of interests.

**Ethical approval** All procedures in studies involving human participants were in accordance with the ethical standards of the institutional and/or national research committee and with the 1964 Declaration of Helsinki and its later amendments or comparable ethical standards.

**Informed consent** For this type of study, formal consent is not required.

**Consent for publication** For this type of study, consent for publication is not required.

## References

1. Chen N, Zhou M, Dong X et al (2020) Epidemiological and clinical characteristics of 99 cases of 2019 novel coronavirus pneumonia in Wuhan, China: a descriptive study. Lancet 395:507–513
2. Zu ZY, Jiang MD, Xu PP et al (2020) Coronavirus Disease 2019 (COVID-19): a Perspective from China. Radiology. https://doi.org/10.1148/radiol.2020200490:200490
3. Wang W, Tang J, Wei F (2020) Updated understanding of the outbreak of 2019 novel coronavirus (2019-nCoV) in Wuhan, China. J Med Virol 92:441–447
4. Tian S, Hu N, Lou J et al (2020) Characteristics of COVID-19 infection in Beijing. J Infect. https://doi.org/10.1016/j.jinf.2020.02.018
5. Huang P, Liu T, Huang L et al (2020) Use of chest CT in combination with negative RT-PCR assay for the 2019 novel coronavirus but high clinical suspicion. Radiology. https://doi.org/10.1148/radiol.2020200330:200330
6. Ai T, Yang Z, Hou H et al (2020) Correlation of chest CT and RT-PCR testing in coronavirus disease 2019 (COVID-19) in China: a report of 1014 cases. Radiology. https://doi.org/10.1148/radiol.2020200642:200642
7. Fang Y, Zhang H, Xie J et al (2020) Sensitivity of chest CT for COVID-19: comparison to RT-PCR. Radiology. https://doi.org/10.1148/radiol.2020200432:200432
8. Bernheim A, Mei X, Huang M et al (2020) Chest CT findings in coronavirus disease-19 (COVID-19): relationship to duration of infection. Radiology. https://doi.org/10.1148/radiol.2020200463:200463
9. Pan F, Ye T, Sun P et al (2020) Time course of lung changes on chest ct during recovery from 2019 novel coronavirus

(COVID-19) pneumonia. Radiology. https://doi.org/10.1148/radiol.2020200370:200370
10. Kanne JP, Little BP, Chung JH, Elicker BM, Ketai LH (2020) Essentials for radiologists on COVID-19: an update-radiology scientific expert panel. Radiology. https://doi.org/10.1148/radiol.2020200527:200527
11. Rawat U, Cohen SL, Levsky JM, Haramati LB (2015) ACR white paper-based comprehensive dose reduction initiative is associated with a reversal of the upward trend in radiation dose for chest CT. J Am Coll Radiol 12:1251–1256
12. Lim HK, Ha HI, Hwang HJ, Lee K (2019) High-pitch, 120 kVp/30 mAs, low-dose dual-source chest CT with iterative reconstruction: prospective evaluation of radiation dose reduction and image quality compared with those of standard-pitch low-dose chest CT in healthy adult volunteers. PLoS One 14:e0211097
13. Bodelle B, Fischbach C, Booz C et al (2017) Free-breathing high-pitch 80kVp dual-source computed tomography of the pediatric chest: image quality, presence of motion artifacts and radiation dose. Eur J Radiol 89:208–214
14. Hagelstein C, Henzler T, Haubenreisser H et al (2016) Ultra-high pitch chest computed tomography at 70 kVp tube voltage in an anthropomorphic pediatric phantom and non-sedated pediatric patients: initial experience with 3(rd) generation dual-source CT. Z Med Phys 26:349–361
15. Johnson TR, Krauss B, Sedlmair M et al (2007) Material differentiation by dual energy CT: initial experience. Eur Radiol 17:1510–1517
16. Marin D, Pratts-Emanuelli JJ, Mileto A et al (2015) Interdependencies of acquisition, detection, and reconstruction techniques on the accuracy of iodine quantification in varying patient sizes employing dual-energy CT. Eur Radiol 25:679–686
17. Krauss B, Grant KL, Schmidt BT, Flohr TG (2015) The importance of spectral separation: an assessment of dual-energy spectral separation for quantitative ability and dose efficiency. Invest Radiol 50:114–118
18. Gordic S, Morsbach F, Schmidt B et al (2014) Ultralow-dose chest computed tomography for pulmonary nodule detection: first performance evaluation of single energy scanning with spectral shaping. Invest Radiol 49:465–473
19. Haubenreisser H, Meyer M, Sudarski S, Allmendinger T, Schoenberg SO, Henzler T (2015) Unenhanced third-generation dual-source chest CT using a tin filter for spectral shaping at 100 kVp. Eur J Radiol 84:1608–1613
20. Chang YC, Yu CJ, Chang SC et al (2005) Pulmonary sequelae in convalescent patients after severe acute respiratory syndrome: evaluation with thin-section CT. Radiology 236:1067–1075
21. Hosseiny M, Kooraki S, Gholamrezanezhad A, Reddy S, Myers L (2020) Radiology perspective of coronavirus disease 2019 (COVID-19): lessons from severe acute respiratory syndrome and middle east respiratory syndrome. AJR Am J Roentgenol. https://doi.org/10.2214/AJR.20.22969:1-5
22. Deak PD, Smal Y, Kalender WA (2010) Multisection CT protocols: sex- and age-specific conversion factors used to determine effective dose from dose-length product. Radiology 257:158–166
23. Mettler FA Jr, Huda W, Yoshizumi TT, Mahesh M (2008) Effective doses in radiology and diagnostic nuclear medicine: a catalog. Radiology 248:254–263
24. Macri F, Greffier J, Pereira FR et al (2016) Ultra-low-dose chest CT with iterative reconstruction does not alter anatomical image quality. Diagn Interv Imaging 97:1131–1140
25. Ludes C, Labani A, Severac F et al (2019) Ultra-low-dose unenhanced chest CT: prospective comparison of high kV/low mA versus low kV/high mA protocols. Diagn Interv Imaging 100:85–93
26. Agostini A, Mari A, Lanza C et al (2019) Trends in radiation dose and image quality for pediatric patients with a multidetector CT and a third-generation dual-source dual-energy CT. Radiol Med 124:745–752